ELSEVIER
CrossMark
Available online at www.sciencedirect.com
ScienceDirect
Procedia Engineering 173 (2017) 1169 – 1176
Procedia Engineering
www.elsevier.com/locate/procedia

11th International Symposium on Plasticity and Impact Mechanics, Implast 2016

Anisotropic large deformation and fatigue damage of rubber-fabric braid layered composite hose

J.R. Cho[a,*]

[a]*Department of Naval Architecture and Ocean Engineering, Hongik University, Jochiwon, Sejong 339-701, Korea*

Abstract

Rubber hoses are widely used in various transport and industrial systems to safely deliver high-pressure working oil without leakage. Usually, those are in a lamination composition of rubber and braided layers to suppress the extreme radial expansion stemming from high internal oil pressure. Braided layers manufactured by fabric or metallic cords are in a complex periodic pattern composed of warp and fill tows, so that those exhibit the inherent anisotropic behavior even though their base cords are isotropic materials. The anisotropy of braided layers causes the out-of-plane deformation of the entire rubber-braid layered composite hose, which becomes more prominent when the composite hose is under the large cyclic motion. A representative example is a braking hose used in automotive hydraulic braking system, in which the hose exhibits the large cyclic dynamic deformation according to the steering and bump/rebound motions of vehicle. The anisotropic large deformation characterized by the out-of-plane deformation in cyclic motion affects not only the hose deformed layout but also the hose durability. Hence, beside the oil-leakage prevention, the deformed layout and durability should be also considered in the design of braided composite hose. Meanwhile, owing to the complex micro structure of braided layers, these two subjects have been traditionally assessed by time- and cost-consuming trial-and-error experiments. In this context, this paper proposes the numerical method for predicting the deformed layout and the fatigue damage by utilizing the large deformation nonlinear finite element analysis. The troublesome braided layers in micro structure are modeled as orthotropic solid by making use of the homogenization method, and the deformed layout was analyzed by the updated Lagrangian method. Meanwhile, the fatigue damage was evaluated by making use of the modified Morrow fatigue model and Minor rule. Using the proposed numerical method, the characteristics of deformed layout and fatigue damage were investigated.

Peer-review under responsibility of the organizing committee of Implast 2016

Keywords: Fabric braid-rubber layered; Composite hose; Anisotropic large deformation; Fatigue damage; Updated Lagrangian formulation; Modified fatigue model

* Corresponding author. Tel.:+82-44-860-2546; fax:+82-41-862-0940.
E-mail address: jrcho@hongik.ac.kr

Peer-review under responsibility of the organizing committee of Implast 2016
doi:10.1016/j.proeng.2016.12.097

Nomenclature

α_H	Helix angle of fabric braided layers
$W(I_1, I_2, I_3)$	Strain energy density functional
κ	Bulk modulus
C_{ij}	Mooney-Rivlin constants
δ_I	Maximum in-plane deformation
δ_O	Maximum out-of-plane deformation
σ_a	Stress amplitude
ε_a	Strain amplitude
ε_m	Mean strain
σ'_f	Fatigue strength coefficient
ε'_f	Fatigue ductility coefficient
b	Fatigue strength exponent
K_f	Fatigue parameter
D_i	Accumulated fatigue damage by the *i*-th strain cycle
$(N_f)_i$	Fatigue life cycle corresponding to the *i*-th strain cycle
N_s	Total number of distinct harmonic strain cycles
n_i	Repetition number of the *i*-th strain cycle
D	Total accumulated fatigue damage
N_f	Fatigue life cycle

1. Introduction

Braking hose shown in Fig. 1(a) in the automotive hydraulic braking system plays an important role of delivering the driver's braking force to the brake disc cylinders via internal working oil. Since the traffic accidents caused by the oil leakage may lead to the fatal casualties, the braking hose should be elaborately designed to prevent the microcraking [1], a main source of oil leakage, during the operation within the whole period of its warranty. The microcraking is mostly attributed to the complicated and large cyclic deformation of hose and to the interference with other adjacent vehicle components. For this reason, the braking hose is in the lamination composition of pure rubber layers and fabric braided layers to effectively prevent the oil leakage and to suppress the excessive large deformation [2,3]. The fabric braided layers are composed of periodic warp and fill tows in the complex pattern, so those exhibit the anisotropic behavior even though their base materials are isotropic material [4-6]. Because of the anisotropic behavior of fabric braided layers, the whole braking hose exhibits the inherent out-of-plane deformation during the steering and bump/rebound motions of vehicle [3]. And, it becomes one of crucial factors in the design of oil leakage-proof high-durable braking hose which produces the interference-free deformed configuration.

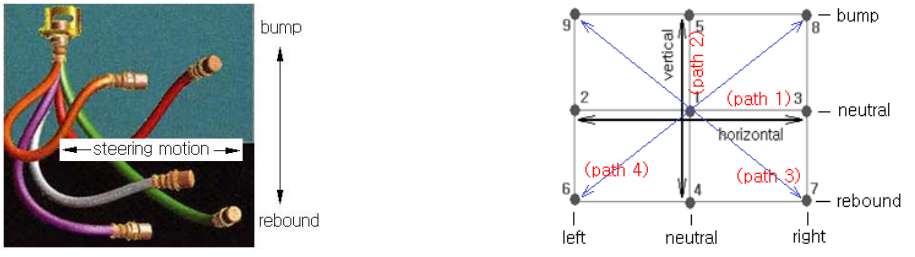

Fig.1 (a) Steering and bump/rebound motions of braking hose, (b) nine extreme positions of defining the cyclic paths

The hose cyclic path is not unique but manifold depending on the combination of the steering and bump/rebound

motions of vehicle [7]. So, a number of major cyclic paths that characterize the hose deformed layout should be identified and numerically interpolated for the numerical simulation. For this reason, the hose deformed configuration for the specific hose cyclic path and the resulting fatigue life have been traditionally evaluated by experiments. However, this approach is highly cost- and time-consuming, and furthermore it leads to the hose layout design of trial and error. To overcome the demerits of experimental approach, the attempts to apply the analytical and numerical methods have been attempted by several investigators. The path of hose movable end for the numerical analysis is not easy to identify because it is diversely determined according to a combination of the tire steering motion and the bump/rebound motion of vehicle.

For this reason, the path is rather simply defined using nine extreme positions shown in Fig. 1(b) that are determined by the tensor product of three positions in the steering mode and three positions in the bump/rebound mode. The neutral position corresponds to the straight driving without bump and rebound, and the left and right positions indicate the maximum steering in the left and right directions. Meanwhile, the bump and rebound indicate the maximum compression and stretching of tire in the vertical direction with respect to the vehicle. Two most representatives are the horizontal path 2-1-3 and the vertical 4-1-5, where the former corresponds to the left-neutral-right handling in cruising while the latter to the center acceleration and braking, respectively. In the current study, four representative cyclic paths defined in Fig. 1(b) are taken for the numerical investigation of hose deformed layout and the fatigue damage.

As an extension of our previous work [3,7] on the braking hose, this paper intends to investigate the characteristics of hose large deformation and fatigue life to the hose cyclic path. Four representative cyclic paths are chosen, and the large deformation and fatigue analyses are carried out for each cyclic path. The homogenization, path interpolation and fatigue evaluation methods are integrated, and the variation of the maximum in-plane and out-of-plane deformations and the critical fatigue life cycles are comparatively investigated.

2. Five-layered rubber-fabric braided composite hose

Fig. 2(a) shows a five-layered reinforced braking hose composed of three rubber layers and two fabric braided layers. The unfold configuration of braided layer is represented in Fig. 2(b), where warp and fill tows are woven with the specific helix angle α_H. Each warp and fill tow are composed of three polyester cords, and the interfaces between warp and fill tows are also assumed to be perfectly bonded. The total number of warp and fill tows within a pitch p is defined by Cr and the diameter of base cord is denoted by *denia* which is defined by the total weight in gram per $9{,}000\,m$ of cord. These material parameters as well as the helix angle are key parameters influencing the anisotropic behavior of braided layer.

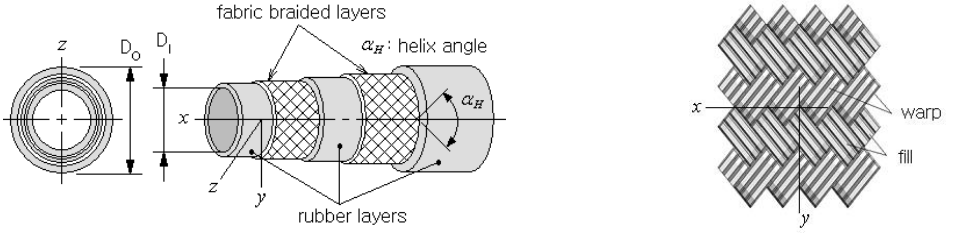

Fig. 2 Fabric braided rubber hose: (a) layer composition, (b) unfolded fabric braid

With the setting of material co-ordinates shown in Fig. 2(a), two fabric braided layers are modeled as an orthotropic material with the constitutive relation [8] given by

$$\{\boldsymbol{\sigma}\} = [\boldsymbol{D}]\{\boldsymbol{\varepsilon}\} \tag{1}$$

with (6×1) stress and strain vectors $\{\boldsymbol{\sigma}\} = \{\sigma_1\,\sigma_2\,\sigma_3\,\tau_{23}\,\tau_{31}\,\tau_{12}\}^T$ and $\{\boldsymbol{\varepsilon}\} = \{\varepsilon_1\,\varepsilon_2\,\varepsilon_3\,\gamma_{23}\,\gamma_{31}\,\gamma_{12}\}^T$. And, the (6×6)

orthotropic material constant matrix $[\boldsymbol{D}]$ contains six diagonal terms defined by $D_{ii}=\left(1-\nu_{jk}\nu_{kj}\right)/E_jE_k\Delta$ and $D_{i+3i+3}=G_{ij}$ and the other six off-diagonal terms defined by

$$D_{ij}=\frac{\nu_{ji}+\nu_{ki}\nu_{jk}}{E_jE_k\Delta}\quad(i\to j\to k),\quad D_{kj}=\frac{\nu_{jk}+\nu_{ik}\nu_{ji}}{E_iE_j\Delta}\quad(k\to j\to i) \tag{2}$$

with $\Delta=\left(1-\nu_{12}\nu_{21}-\nu_{23}\nu_{32}-\nu_{31}\nu_{13}-2\nu_{12}\nu_{23}\nu_{31}\right)/E_1E_2E_3$. Where, subscripts 1, 2 and 3 stand for x, y and z.

Meanwhile, the incompressible hyperelastic behavior of three rubber layers is modeled by a four-term Mooney-Rivlin material model [9] which is expressed by the strain energy density functional $W\left(I_1,\ I_2,\ I_3\right)$ defined by

$$W\left(I_1,I_2,I_3\right)=C_{10}\left(I_1-3\right)+C_{01}\left(I_2-3\right)+C_{20}\left(I_1-3\right)\left(I_2-3\right)+\frac{\kappa}{2}\left(I_3-1\right)^2 \tag{3}$$

In which, I_i are the invariants of Green-Lagrange strain tensor, κ the bulk modulus, and C_{ij} the material dependent Mooney-Rivlin constants. The incompressibility of rubber is enforced by the last term on the right hand side of Eq. (3). The Mooney-Rivlin constants which were determined by the uniaxial tension test of rubber specimen are given in Appendix.

3. Evaluation of hose deformation and fatigue damage

3.1. Deformation measurement

The layout design of braking hose based on the deformed configuration is an important subject because the sliding contact of the braking hose with other adjacent vehicle parts wears down the outer rubber layer. The continuation of such wearing down not only weakens the structural strength of hose but also causes the fatal oil leakage. However, the layout design has been traditionally performed based on the trial and error experiments because the complex anisotropic hose deformation cannot be accurately analyzed by the conventional simple isotropic hose model as mentioned earlier. In fact, the layout design is a troublesome task because the hose deformed configuration is path-dependent and continuously varying with the hose movement. In other words, the designer should evaluate a huge amount of deformation data at every moving stage on various hose paths, in order to extract the characteristic deformation magnitude that will be used for the layout design.

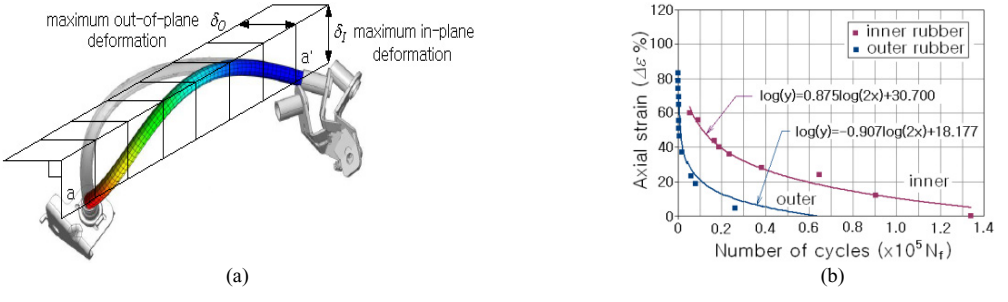

Fig. 3. (a) Maximum in-plane and out-of-plane deformations; (b) $\varepsilon-N$ curves of two rubber layers

In this regard, the numerical approach employing an appropriate anisotropic hose model can successfully resolve the above-mentioned problems of the traditional experiment-based layout design, because it can accurately and quickly obtain and evaluate the hose deformation data for various hose paths. Meanwhile, the choice of characteristic deformation magnitude depends on the design standards of car maker, but we in this study choose two maximum principal deformations to investigate the deformation configuration to the hose path. Referring to Fig. 3(a), one is the maximum in-plane deformation and the other is the maximum out-of-plane deformation, and the

both are measured with respect to the straight line $a-a'$ connecting two hose ends. The largest normal distance between the deformed hose and the straight line always becomes the maximum in-plane deformation, while the other on the plane normal to the in-plane becomes the maximum out-of-plane deformation.

3.2. Modified fatigue model

The cyclic motion of braking hose along a specific path produces the complex cyclic variations of strains and stresses, with the presence of mean strain and stress that are resulted from the pre-deformation that was caused when the braking hose is assembled at the neutral position. When the applied stresses generate predominantly elastic strain amplitudes, the mean stress effect can be taken into consideration by Basquin's mean stress correction method [10,11] given by $\sigma_{ar}=\sigma'_f\left(2N_f\right)^b$, where N_f is the fatigue life, σ'_f the fatigue strength coefficient, and b the fatigue strength exponent, respectively. Here, $\sigma_{ar}\left(=\sqrt{\sigma_{max}\sigma_a}\right)$ denotes the equivalent fully reversed stress amplitude defined in terms of the maximum stress σ_{max} and the stress amplitude σ_a. But, when the cyclic response of the material is within the elastic-plastic stress-strain range, the mean stress effect on fatigue life is based on the strain-life approach represented by

$$\frac{\Delta\varepsilon}{2}=\varepsilon_a=\frac{\Delta\varepsilon^e}{2}+\frac{\Delta\varepsilon^p}{2}=\frac{\sigma'_f}{E}\left(2N_f\right)^b+\varepsilon'_f\left(2N_f\right)^c \tag{4}$$

where ε_a is the strain amplitude, ε'_f the fatigue ductility coefficient, and c the fatigue ductility exponent. The modification of Eq. (4) which is used to predict the fatigue life for zero mean stress was made by several investigators [12,13]. The current study utilizes the Morrow model given by

$$\frac{\Delta\varepsilon}{2}=\frac{\sigma'_f-\sigma_m}{E}\left(2N_f\right)^b+\varepsilon'_f\left(2N_f\right)^c \tag{5}$$

By the way, this correction model is needed to be slightly modified for the current study because the large deformation analysis of braking hose is carried out using the Moonley-Rivlin hyperelastic material model by neglecting the plastic strain. Furthermore, the term σ'_f/E is replaced with a material-dependent fatigue parameter K_f which can be determined from the $\varepsilon-N$ curves shown in Fig. 3(b) in the log-log scale. Then, we have the modified Morrow model given by

$$\frac{\Delta\varepsilon}{2}=\left(K_f-\varepsilon_m\right)\left(2N_f\right)^b \tag{6}$$

Since strains and stresses at each material point exhibit the complex time histories composed of a number of harmonic cycles, as illustrated in Fig. 5(b), we employ the Palmgren-Minor cumulative damage law [14] given by

$$D=\sum_{i=1}^{N_s}D_i,\quad D_i=\frac{n_i}{\left(N_f\right)_i} \tag{7}$$

to calculate the total accumulated fatigue damage D during a single deformation cycle along the specific cyclic path. Here, N_s is the total number of distinct harmonic strain cycles, D_i the accumulated fatigue damage by the i-th harmonic strain cycle, and n_i and $\left(N_f\right)_i$ the repetition number and the fatigue life of the i-th strain cycle, respectively. Then, the fatigue life $N_f\left(cycles\right)$ at each material point within the braking hose along the specific path is calculated by $N_f=1/D$. The fatigue life calculation is performed node by node using the signed nodal von Mises strains $\pm\varepsilon_{vm}$. The repletion numbers n_i of each distinct strain cycle are counted by the rainflow cycle counting method.

4. Numerical results

A five-layered braking hose of the length L of $230mm$ and the outer diameter D_o of $10.5mm$ is taken for the numerical experiments. The top end is clamped while the bottom end is forced to move along the predefined cyclic path, where the center co-ordinates and rotations of the cross-section of the bottom end at nine extreme positions are referred to our previous paper [7]. Referring to the previous Fig. 2(a), the thicknesses of five layers are as follows: $1.25, 0.30$ and $1.10mm$ for the outer, middle and inner rubber layers and $0.45mm$ for the outer and inner fabric braided layers. Two fabric braided layers are manufactured with PVA (poly vinyl alcohol) and the helix angles α_H, pitch p and C_r are as follows: 53.64^o, $18.5mm$ and 24 for the outer layer and 55.57^o, $14.0mm$ and 20 for the inner layer. The homogenized orthotropic material properties of the inner and outer fabric braided layers are given in Appendix.

Three rubber layers are manufactured with EPDM (ethylene-propylene-diene-monomer), and the fatigue life is evaluated for the outer and inner rubber layers because both layers are weak to fatigue damage and play an important role in preventing the oil leakage. The entire braking hose is uniformly discretized with the total of 33,002 8-node hexahedron elements. Basically, the updated Lagrangian formulation is used to compute the increments of strain and stress during the hose large deformation along the cyclic path, and the invariants of Green-Lagrange strain tensor in Mooney-Rivlin models were evaluated in the sense of total Lagrangian. Two fatigue parameters K_f and b in the modified Morrow model in Eq. (6) are found to be: 30.7003 and -0.8754 for the inner rubber layer and 18.1773 and -0.9067 for the outer rubber layer, respectively.

Fig. 4 represents the in-plane and out-of-plane deformations of the braking hose for four different paths when their deformations reach the peak values. It is clearly observed that the deformed layouts and the maximum values δ_I and δ_O are quite different for different paths. Paths 1 and 3 produce relatively larger in-plane deformations, but conversely, the out-of-plane deformations at both paths are shown to be insignificant. In case of the out-of-plane deformation, it is shown to be remarkable at paths 2 and 4. As given in Table 1, the maximum in-plane and out-of-plane deformations are largest at path 1 and 2, respectively, such that δ_I is $71.59mm$ while δ_O is $17.75mm$. This comparative investigation confirms the importance of deformation analysis for the hose layout design to avoid the interference with other adjacent automotive parts.

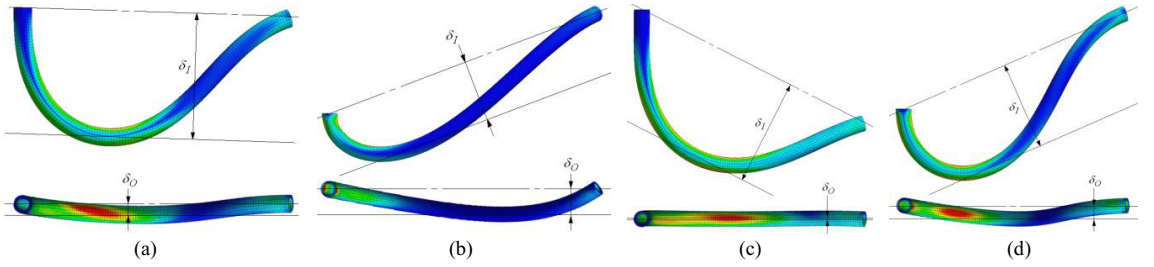

Fig. 4. Maximum in- and out-of-plane plane deformations: (a) path 1, (b) path 2, (c) path 3, (d) path 4.

Table 1. Comparison of the hose deformations, the peak equivalent strains and stresses, and the critical fatigue lives to the cyclic path.

Items		Cyclic paths			
		1	2	3	4
Maximum deformation (*mm*)	In-plane	71.59	41.66	70.01	59.52
	Out-of-plane	6.67	17.75	0.95	9.43
Peak equivalent strain		0.582	0.287	0.466	0.144
Peak effective stress (*MPa*)		4.992	2.485	5.664	1.142
Critical fatigue life (*Cycles*)	Outer rubber	4,806	21,623	5,735	12,412
	Inner rubber	45,657	133,765	54,482	168,151

The maximum in-plane and out-of-plane deformations, the peak equivalent strains and stresses and the critical fatigue lives for four different paths are given in Table 1. It is found that both the peak equivalent strain and stress are remarkable at paths 1 and 3, which is because both paths produce relatively larger deformations as shown in Fig. 4. Meanwhile, for all the paths, it is observed that the significantly high strain and stress are produced in the upper one-third region and in the vicinity of lower movable end. It is because the deformation in these regions is characterized by the combined bending and torsion as well as the extension, differing from the intermediate region showing the relatively simple and small deformation. The peak equivalent strain 0.582 is occurred in the vicinity of the upper fixed end at path 1, while the peak effective stress $5.664MPa$ appears at the same point but at path 3.

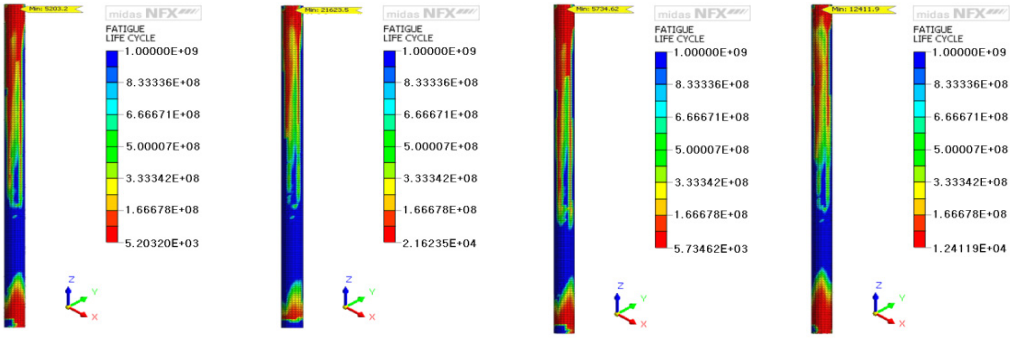

(a) (b) (c) (d)

Fig. 5. Fatigue life profiles of the outer rubber layer: (a) path 1, (b) path 2, (c) path 3, (d) path 4

Fig. 5 comparatively represent the path-wise fatigue life profiles of the outer rubber layer. It is observed that all the cases show the remarkably lower fatigue lives in the vicinity of upper fixed and lower movable ends because the equivalent strain is relatively larger in these regions. It implies that the durability of barking hose is determined by these regions, and its improvement could be possible only when the strain level in these regions is reduced. Regarding the hose path, it is found that the critical fatigue life is significantly lower at paths 1 and 3 when compared with paths 2 and 4. As given in Table 1, path 1 shows the lowest critical fatigue life cycle equal to 4,806 in the vicinity of upper fixed end. Thus, from the comparative numerical results of the hose deformation and fatigue life, it is found that paths 1 and 3, particularly path 1, should be considered importantly for the layout and durability design of braking hose.

5. Conclusion

The deformed layout and the fatigue life cycle of five-layered rubber-fabric braided composite hose were numerically investigated with respect to four representative cyclic paths. The anisotropic behavior of fabric braided layers in micro structure was modeled as an orthotropic solid, and the hose cyclic paths were numerically interpolated using their nine extreme positions. The fatigue damage that is accumulated along the cyclic motion was evaluated by the modified Morrow fatigue model. Through the numerical experiments, it has been found that both the deformed layout and the critical fatigue life cycle are significantly dependent of the cyclic path. It is observed that the maximum in-plane deformation is largest at path 1 while the maximum out-of-plane deformation is prominent at path 2. Meanwhile, the critical fatigue life cycles were observed at the outer rubber layer for all the cyclic paths, and the lowest critical fatigue life was occurred at path 1. Thus, from the comparative numerical experiments, it has been found that the hose layout and durability design should be made based on cyclic path 1.

Acknowledgements

This research was supported by Basic Science Research Program through the National Research Foundation of

Korea (NRF) funded by the Ministry of Education (Grant No. NRF-2014R1A1A2055820).

Appendix: Material properties

Table A1. Mooney-Rivlin constants and bulk modulii of rubber layers [7].

Rubber layer	C_{10}	C_{01}	C_{20}	κ
Inner	-1.86902	4.18478	0.41739	1,744.02150
Middle	0.15109	-0.14348	0.38478	7.84270
Outer	-2.46630	4.74565	0.48043	1,225.42264

Table A2. Homogenized orthotropic material properties of fabric braided layers [3].

	Young's modulus (N/mm^2)			Poison's ratio			Shear Modulus (N/mm^2)		
	E_1	E_2	E_3	ν_{12}	ν_{23}	ν_{31}	G_{12}	G_{23}	G_{31}
Outer	819.2	733.1	1,128.4	0.05	0.16	0.16	14.6	6,490.8	8,241.5
Inner	915.3	801.0	1,547.1	0.03	0.15	0.18	17.8	6,832.7	8,816.2

References

[1] S.B. Kwack, N.S. Choi, Micro-damage formation of a rubber hose assembly for automotive hydraylic brakes under a durability test, Eng. Fail. Anal. 16(4) (2009) 1262-1269.
[2] K.M. Entwistle, The behavior of braided hydraulic hose reinforced with steel wires, Int. J. Mech. Sci. 23 (1981) 229-241.
[3] J.R. Cho, Y.B. Jee, W.J. Kim, S.R. Han, S.B. Lee, Homogenization of Braided Fabric Composite for Reliable Large Deformation Analysis of Reinforced Rubber Hose, Composites: Part B 53, (2013) 112-120.
[4] J.R. Cho, J.I. Song, J.H. Choi, Prediction of effective mechanical properties of reinforced braid by 3-D finite element analysis, Key Eng. Mater. 306-308 (2006) 799-804.
[5] L. Xu, S.J. Kim, C.H. Ong, S.K. Ha, Prediction of material properties of biaxial and triaxial braided textile composites, J. Composite Mater. 46(18) (2012) 2255-2270.
[6] M. Chuda-Kowalska, A. Garstecki, Experimental study of anisotropic behavior of PU foam in sandwich panels, *Steel Comp. Struct.* **20**(1) (2016) 43-56.
[7] J.R. Cho, Y.H. Yoon, C.W. Seo, Y.G. Kim, Fatigue life assessment of fabric braided composite rubber hose in complicated large deformation cyclic motion, Finite Elem. Anal. Des. 100 (2015) 65-76.
[8] I.M. Daniel, O. Ishai, Engineering Mechanics of Composite Materials, Oxford University Press, New York, 1994.
[9] R.S. Rivlin, Large elastic deformations of isotropic materials. IV. Further developments of the general theory, Philosophical Transactions of the Royal Society of London. Series A, Math. Phys. Sci. 241(835) (1948) 379-397.
[10] O.H. Basquin, The exponential law of endurance tests, Proc. Am. Soc. Test. Mater. 10 (1910) 625-630.
[11] A. Karolczuk, M. Kowalski, R. Bariski, F. Zok, Fatigue phenomenon in explosively welded steel-titanium clad components subjected to push-pull loading, Int. J. Fatigue 48 (2013) 101-108.
[12] K.N. Smith, P. Watson, T.H. Topper, A stress-strain function for the fatigue of materials, J. Mater. 5 (1970) 767-778, 1970.
[13] A. Ince, G. Glinka, A modification of Morrow and Smith-Watson-Topper mean stress correction models, Fatigue Fract. Eng. Mater. Struct. 34(11) (2011) 854-867.
[14] A. Palmgren, Die lebensdaur von Kugellagren, Zeitschr VDI 69 (1924) 339-341.